IEEE Access
Multidisciplinary | Rapid Review | Open Access Journal

Received January 5, 2021, accepted January 13, 2021, date of publication January 18, 2021, date of current version January 25, 2021.

Digital Object Identifier 10.1109/ACCESS.2021.3052165

Modeling and Optimization of Compensating Oil Viscous Power for a Deep-Sea Electric Manipulator

YUNFEI BAI[1,2,3,4], QIFENG ZHANG[1,2,3], AND AIQUN ZHANG[1,2,3]

[1]State Key Laboratory of Robotics, Shenyang Institute of Automation, Chinese Academy of Sciences, Shenyang 110016, China
[2]Institutes for Robotics and Intelligent Manufacturing, Chinese Academy of Sciences, Shenyang 110169, China
[3]Key Laboratory of Marine Robotics, Liaoning Province, Shenyang 110169, China
[4]Department of Mechatronic Engineering, University of Chinese Academy of Sciences, Beijing 100049, China

Corresponding author: Qifeng Zhang (zqf@sia.cn)

This work was supported by the National Key Research and Development Project under Grant 2017YFC0306402 and Grant 2016YFC0300400.

ABSTRACT The dynamic performance and load capacity of a deep-sea electric manipulator are obviously affected by the viscous resistance of compensating oil. However, the complex geometric clearance of the oil-filled joint of the manipulator makes it difficult for existing theoretical models to accurately model this problem. Based on the existing theoretical models, a viscous power model considering the influence of the surface grooves of the rotor and stator is proposed. To reduce the viscous power loss, an optimization method for the clearance geometry is proposed. This optimization method is carried out by filling the surface grooves of the motor rotor and stator with epoxy resin. This method makes the clearance geometry of the compensated oil more regular. The modified model and optimization method are validated by designing an experimental installation and method. The experimental results demonstrate the accuracy and effectiveness of the modified theoretical model and optimization method.

INDEX TERMS Compensating oil viscous power, deep-sea electric manipulator, modified modeling, viscous power experiment, viscous power optimization.

I. INTRODUCTION

As it is difficult for humans to adapt to the deep-sea environment, underwater robots have become an important means to explore the deep sea on behalf of humans. Unmanned underwater vehicles (UUVs) can be classified as remotely operated underwater vehicles (ROVs), autonomous underwater vehicles (AUVs) and underwater gliders. Conventional AUVs and underwater gliders do not have the ability to carry out operations. ROVs are capable of operating underwater but require expensive mothership support. To meet the requirements of low-cost operation, hybrid underwater vehicles have been studied, and they have been noted as an important research direction for future underwater vehicles [1], [2]. The typical representatives are the full deep-sea autonomous and remotely operated vehicle (ARV) studied at the Shenyang Institute of Automation of the Chinese Academy of Sciences and the TRIDENT interventional AUV (I-AUV) studied by the European Union [3], [4]. Both types of underwater vehicle carry a power source and can perform underwater operations autonomously without the need for expensive mothership support (Fig. 1).

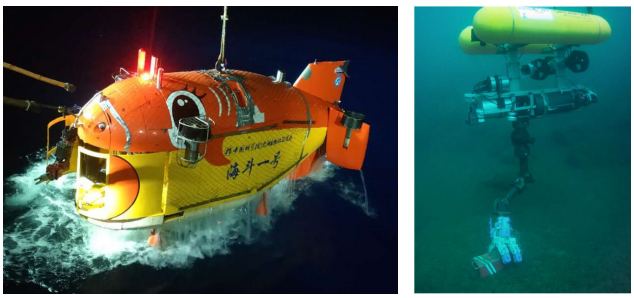

FIGURE 1. The full deep-sea autonomous and remotely operated vehicle and the TRIDENT interventional AUV.

Robots usually use manipulators to operate and retrieve underwater objects [5]–[7]. An underwater electric

The associate editor coordinating the review of this manuscript and approving it for publication was Camelia Delcea.

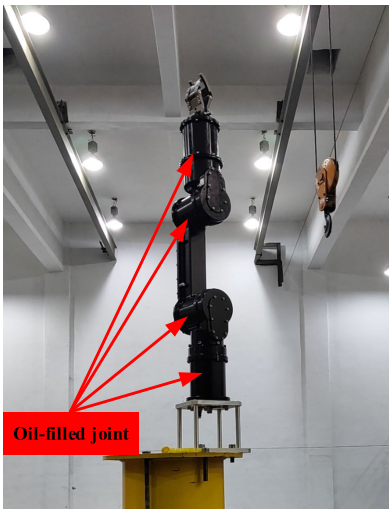

FIGURE 2. Deep-sea electric manipulator.

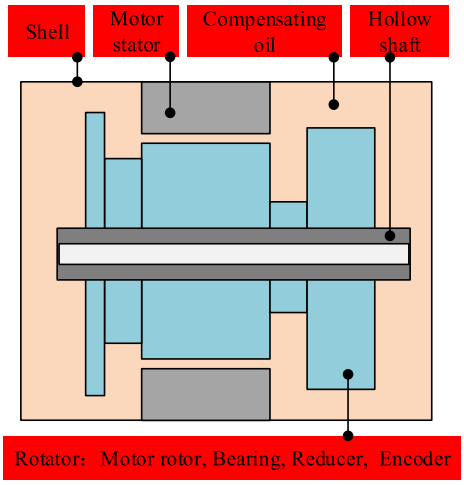

FIGURE 3. Schematic diagram of the oil-filled joint of a deep-sea electric manipulator.

manipulator has the characteristics of low power consumption, a light weight and high precision [8]. Therefore, a hybrid underwater vehicle is usually equipped with an electric manipulator to complete underwater operations. A deep-sea electric manipulator is shown in Fig. 2. The deep-sea electric manipulator has four degrees of freedom and a clamp function. It operates at a depth of 3,000 meters.

Due to the high water pressure in the deep-sea environment, the deep-sea electric manipulator balances the seawater pressure with compensating oil to prevent the shell from bearing great pressure in one direction. The compensating oil is usually insulated. However, the low temperature and high pressure of the deep-sea environment lead to a significant increase in the viscosity of the compensating oil, subjecting the joint driving motor in the oil to a greater viscous friction resistance. As shown in Fig. 3, the rotator of the oil-filled joint of the deep-sea electric manipulator includes the motor rotor, bearing, reducer, and Hall sensor and encoder. The complex clearance between the rotator and the motor stator and shell is filled with compensating oil.

When the rotator rotates in the oil, it drives the oil to rotate as well. Due to the presence of a viscous shear force, a viscous resistance moment will act on the rotator, reducing the actual output efficiency of the joint. The dynamic model of the oil-filled joint considering the viscous moment is as follows:

$$\boldsymbol{\tau}_{\mathrm{J}} = i\eta(\boldsymbol{\tau}_{\mathrm{M}} - \boldsymbol{\tau}_{\mathrm{V}}) \tag{1}$$

where $\boldsymbol{\tau}_{\mathrm{J}}$ stands for the joint output torque, i stands for the reduction ratio of the reducer, $\boldsymbol{\eta}$ stands for the transmission efficiency of the reducer, $\boldsymbol{\tau}_{\mathrm{M}}$ stands for the output torque of the motor and $\boldsymbol{\tau}_{\mathrm{V}}$ stands for the moment of viscous friction. It can be seen from the formula that the compensating oil viscous moment is applied directly to the motor rotor rather than to the output end after the reducer. Even a small viscous friction moment will significantly reduce the joint output efficiency. Previous studies and experiments by the research group [9], [10] showed that the viscous friction power of the oil-filled joint accounts for a large part of the output power of the motor and that it increases exponentially with the increase in oil viscosity. Therefore, viscous power modeling and optimization of deep-sea electric manipulators are of great significance and are nonnegligible components of deep-sea electric manipulator dynamics modeling [11], [12].

Our main contributions are summarized as follows:

- Based on the existing theoretical model, a modified theoretical model is proposed for the complex clearance geometry in the oil-filled joints of deep-sea electric manipulators. The modified theoretical model considers the influence of the surface grooves of the motor stator and rotor on the viscous power. The experimental results show that the modified theoretical model has clearly higher accuracy.
- The viscous power is unnecessary power that reduces the driving efficiency of the manipulator joint. In this paper, a method of smoothing the surface grooves of the rotor and stator is presented to optimize the viscous friction power. The experimental results show that this optimization method can significantly reduce the viscous power loss and that the optimization method has little effect on the joint inertia.
- Finally, an experimental installation to study the viscous power in an oil-filled joint is established, and a reasonable experimental method is designed. The modified model and optimization method are validated by experiments.

The remainder of the paper is organized as follows: in section II, the existing modeling methods are introduced, and then a modified theoretical modeling method is proposed. An optimization method for reducing the viscous friction power is proposed in section III. Section IV gives the experimental process and results. The paper is concluded in section V.

II. THEORETICAL MODELING OF VISCOUS POWER

A simplified physical model of the oil-filled joint of a deep-sea electric manipulator is the concentric cylinder model, which is a classic study case (Taylor-Couette flow) in fluid mechanics. The characteristics of fluid velocity, temperature and force in the clearance of the concentric cylinders are studied. The viscous resistance moment generated by the fluid viscosity between two cylinders is expressed as [13]:

$$\tau_{\mathrm{v}} = 4\pi\mu \frac{R_1^2 R_2^2}{R_2^2 - R_1^2} (\dot{q}_2 - \dot{q}_1) \tag{2}$$

where μ is the kinematic viscosity of the oil, R_1 and R_2 represent the outer diameter of the inner cylinder and inner diameter of the outer cylinder, respectively, and $\dot{q}_1$ and $\dot{q}_2$ represent the angular velocity of the inner cylinder and the outer cylinder, respectively.

Formula (2) is applicable to the calculation of the viscous moment when the state of the Taylor-Couette flow is laminar flow. When the angular velocity of rotation, oil viscosity and clearance size change, the Taylor-Couette flow gradually changes to a turbulent state, and formula (2) is no longer applicable [14]. The Taylor number [15] can be used to judge the flow state. The Taylor number is defined as:

$$T_a = \mathrm{Re}\left(\frac{\delta}{R}\right)^{0.5} \tag{3}$$

where $\mathrm{R_e}$ is the Couette-Reynolds number:

$$\mathrm{Re} = \frac{\dot{q} R \delta}{\mu} \tag{4}$$

where $\dot{q}$ denotes the angular velocity of the rotation and R denotes the radius of the rotation. The relevant literature [14], [16] shows that when the Taylor number is greater than 41.3, the flow pattern of Taylor-Couette flow gradually changes from laminar to turbulent flow, and the change in the flow pattern will obviously lead to a change in the viscous power. Reference [17] gives the equation for the viscous moment when the Taylor number is greater than 41.3 and less than 400. Reference [18] gives the equation for the viscous moment when the Taylor number is greater than 400. Reference [19] analyzes and summarizes the above equations in different flow patterns and gives a comprehensive equation for the viscous power in different flow patterns:

$$p_v = 0.5\pi C_m \rho \dot{q}^3 R^4 L \tag{5}$$

where ρ is the fluid density and L denotes the length of the rotation. The viscous coefficient is calculated in $\mathrm{R_e}$ stages as follows:

$$C_m = \begin{cases} 10.0\,\mathrm{Re}^{-1}\left(\frac{\delta}{R}\right)^{0.3} & for\ \mathrm{Re} < 64 \\ 2.00\,\mathrm{Re}^{-0.6}\left(\frac{\delta}{R}\right)^{0.3} & for\ 64 \le \mathrm{Re} < 500 \\ 1.03\,\mathrm{Re}^{-0.5}\left(\frac{\delta}{R}\right)^{0.3} & for\ 500 \le \mathrm{Re} < 10000 \\ 0.065\,\mathrm{Re}^{-0.2}\left(\frac{\delta}{R}\right)^{0.3} & for\ 10000 \le \mathrm{Re} \end{cases} \tag{6}$$

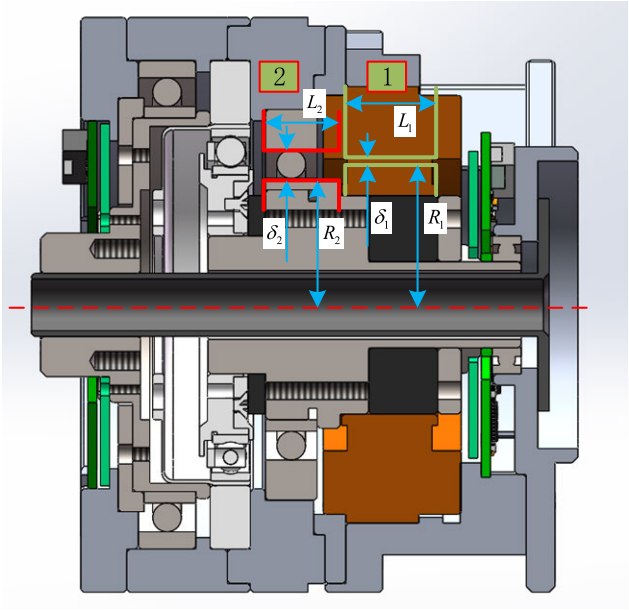

FIGURE 4. Sectional view of the oil-filled joint of a deep-sea electric manipulator.

The relationship between the viscous coefficient C_m and the dimensionless parameter of the clearance width δ/R and Couette-Reynolds number $\mathrm{R_e}$ is a power function, where C represents the proportional coefficient. The general equation of the viscous coefficient C_m is:

$$C_m = C\left(\frac{\delta}{R}\right)^{\alpha} \mathrm{Re}^{\beta} \tag{7}$$

where α and β are determined according to (6).

Fig. 4 shows a sectional view of the manipulator drive module, in which the viscous power loss is mainly generated in regions 1 and 2. Region 1 is the motor stator and rotor, and the clearance between the rotor and stator is filled with compensating oil. Region 2 is mainly the inner ring and outer ring of the bearing. The clearance between the inner ring and outer ring is filled with compensating oil, and the inner ring rotates at a high speed with the motor rotor. The physical geometry of these two regions can be reduced to the green and red boxes shown in the figure, where δ_1 and δ_2 represent the width of the clearance in the two fluid regions, L_1 and L_2 represent the length of the two fluid regions, and R_1 and R_2 represent the radius of the rotation in the two fluid regions.

The viscous friction power consumption of the oil-filled joints of a deep-sea manipulator is mainly generated by regions 1 and 2. The viscous power generated by region 2 can be calculated by formulas (5) and (6). In the classical physical model of a concentric cylinder in fluid mechanics, the surface of the cylinder is considered to be smooth, so there is no parameter to represent the geometric roughness of the cylinder surface in formulas (5) and (6). The stator and rotor surfaces of the motor in region 1 are covered in grooves, and the roughness of the surface geometry affects the viscous power. To describe the viscous power of region 1 more accurately, the general equation for the viscosity

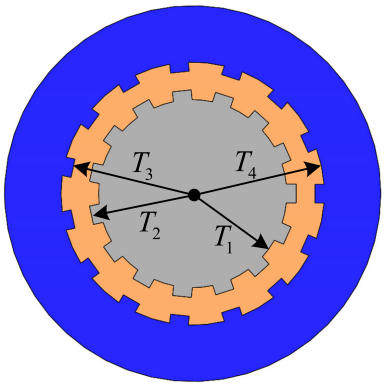

FIGURE 5. Geometric model of the clearance between the rotor and stator.

coefficient of (7) is modified as follows:

$$C_m = C\left(\frac{\delta}{R}\right)^{\alpha} \mathrm{Re}^{\beta}(T)^{\gamma} \tag{8}$$

where T represents the geometric roughness of the clearance between the motor rotor and stator and is defined as follows:

$$T = \frac{T_4 - T_1}{T_3 - T_2} \tag{9}$$

where T_1, T_2, T_3 and T_4 represent the geometric parameters of the motor rotor and stator, as shown in Fig. 5. The closer the geometric roughness T is to 1, the smoother the clearance between the rotor and stator. The modified viscosity coefficient C_m is a power function of the clearance width parameter, the Couette-Reynolds number and the clearance geometry roughness, and it is more suitable for the calculation of the viscous power of region 1.

In summary, the viscous power model of the deep-sea manipulator is as follows:

$$p_v = p_{v1} + p_{v2} = 0.5\pi\rho\dot{q}^3\left(C_{m1}R_1^4L_1 + C_{m2}R_2^4L_2\right) \tag{10}$$

where p_{v1} and p_{v2} denote the viscous power of region 1 and region 2, respectively, and C_{m1} and C_{m1} denote the viscosity coefficient of region 1 and region 2, respectively. C_{m1} can be calculated from (8), and C_{m2} can be calculated from (7).

III. VISCOUS LOSS POWER OPTIMIZATION

Some studies improve the driving ability of deep-sea oil-filled motors by designing a special underwater motor. The coupling calculation of the flow state and temperature of the underwater oil-filled motors is carried out in reference [20]. Reference [21] studies the design method of oil-filled motors considering the influence of high water pressure in the deep sea. Reference [22] studies the influence of the deep-sea low-temperature and high-pressure environment on oil-filled motors. However, the design of a special deep-sea oil-filled motor requires professional knowledge and incurs a high cost. In contrast, this paper uses a simple method to optimize the driving capacity of deep-sea motors.

Viscous power is unnecessary power that reduces the output efficiency of the manipulator joint. Therefore, the viscous power can be optimized by finding ways to reduce the influence of viscous power. The viscous power can be optimized through two methods. The first is to use a compensating oil with lower viscosity or a compensating oil that is less affected by the deep-sea temperature and pressure, but this may cause problems such as leakage and poor lubrication. The second method is to improve the geometric characteristics of fluid clearance. Equations (8) and (9) show that the grooves on the surface of the motor stator and rotor increase the viscous resistance. In this paper, the viscous power is reduced by smoothing the grooves.

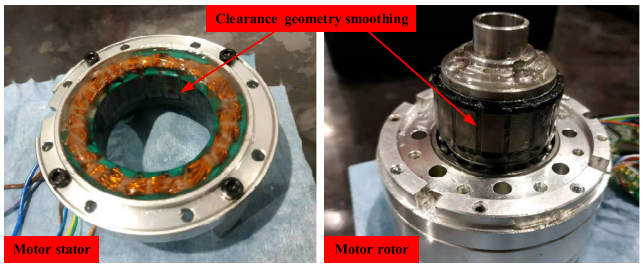

FIGURE 6. Motor stator and rotor surface smoothing.

The motor rotor and stator after smoothing are shown in Fig. 6. The smoothing process is achieved by using epoxy resin to fill the grooves evenly to make the compensated oil clearance more regular. The stator coil surface is also smoothed. Epoxy resin is used as a filler because it has good pressure resistance and can maintain a smooth appearance under high water pressure. Because of the low density of epoxy resin, the effect on the rotor inertia of the epoxy resin coating in the rotor groove can be ignored.

By coating the grooves on the stator and rotor surfaces with epoxy resin, the parameters T_1 and T_4 in Fig. 5 are changed. T_1 is closer to T_2, and T_4 is closer to T_3. Smooth optimization reduces the geometric roughness of the clearance between the motor rotor and stator. Formula (9) is used to calculate the geometric roughness of the clearance before the smooth processing as follows: $T_a = 4$. The geometric roughness of the clearance after smooth processing is $T_b = 2$. The smooth processing changes only the viscous power of region 1 but not the viscous power of region 2. The viscous power before smooth processing is

$$p_{va} = p_{va1} + p_{v2} = 0.5\pi\rho\dot{q}^3\left(C_{ma1}R_1^4L_1 + C_{m2}R_2^4L_2\right) \tag{11}$$

where C_{ma1} is the viscosity coefficient of region 1 before smooth processing.

The viscous power after smooth processing is

$$p_{vb} = p_{vb1} + p_{v2} = 0.5\pi\rho\dot{q}^3\left(C_{mb1}R_1^4L_1 + C_{m2}R_2^4L_2\right) \tag{12}$$

where C_{mb1} is the viscosity coefficient of region 1 after smooth processing.

After smooth processing, the viscous power decreases by

$$\Delta p_v = p_{vb} - p_{va} = 0.5\pi\rho\dot{q}^3R_1^4L_1\left(C_{mb1} - C_{ma1}\right) \tag{13}$$

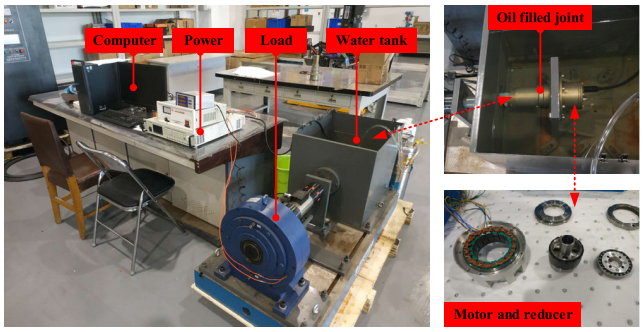

FIGURE 7. Composition of the experimental installation.

IV. EXPERIMENT OF VISCOUS POWER

A. EXPERIMENTAL INSTALLATION

The experimental installation composition is shown in Fig. 7. The experimental object is the oil-filled joint module of the deep-sea electric manipulator, which is mainly composed of a frameless motor and a harmonic reducer. During the experiment, it is placed in a tank to simulate the underwater heat dissipation environment. An adjustable load applies a constant torque to the joint. The oil-filled joint is supplied with 48 V by the DC power supply and communicates with the computer through a controller area network bus. The oil-filled joint receives the computer's control instructions and feeds back the angular velocity information of the motor. The computer communicates with the DC power supply through the RS232 to obtain the output power information. The computer can save the motor and power information in data files.

The deep-sea manipulator drive motor is a frameless motor. The motor rotor and stator are separated and there is no shell. The rated speed of the motor is 3000 rpm. The geometric parameters of the two fluid regions in Fig. 4 are shown in Table 1.

TABLE 1. Geometric parameters of the viscous fluid region.

Region 1 /mm			Region 2 /mm		
R_1	L_1	δ_1	R_2	L_2	δ_2
25.4	14.76	1	22	14.24	5

B. EXPERIMENTAL METHOD

The viscosity of the compensating oil of the deep-sea electric manipulator changes significantly with the change in the underwater pressure and temperature. In underwater conditions at approximately 2 ° and 7000 m depth, the kinematic viscosity of #22 shell hydraulic oil is approximately 857 cSt. To simulate the actual working conditions in the deep sea and simplify the experimental installation, high-viscosity oil was selected as the compensating oil under normal temperature and pressure to simulate the viscosity of oil in the deep sea. Table 2 shows the kinematic viscosity (measured at 40° and normal pressure) of four kinds of oil selected for the experiment. The experiment is divided into 5 groups, numbered from 0 to 4, among which group 0 is the oil-free group.

TABLE 2. Experimental group design.

Experimental group number	Compensating oil viscosity /cSt
0	oil-free
1	150
2	320
3	680
4	1000

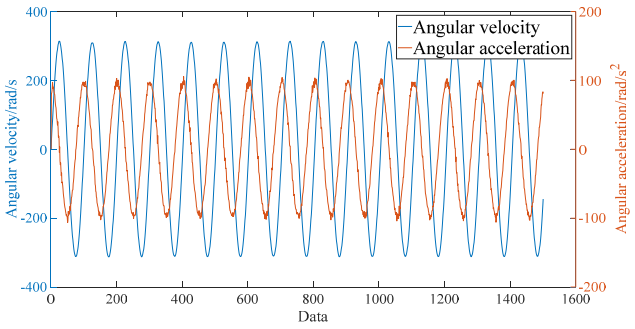

FIGURE 8. Angular velocity and angular acceleration of the motor.

Each experiment lasts for 5 min, and the data sampling interval is 200 ms. Each experimental group includes 1500 data points.

In the 5 groups of experiments, the angular velocity of the motor is $\dot{q} = 3000\sin(0.1\pi t)$. The peak angular velocity is 3000 rpm ($\approx$ 314.16 rad/s), which is the rated velocity of the motor. The frequency of the velocity changes is 0.05 Hz. Such velocity changes yield more comprehensive experimental information. The feedback signals of the angular velocity and angular acceleration of the actual motor are shown in Fig. 8.

The kinematic viscosity of the four kinds of compensating oil selected in the experiment is measured at a temperature of 40° under normal pressure. In the actual experiment, the viscosity of the oil changes with the temperature. The heat generated by the motor rotation causes the temperature to increase rapidly at the beginning of the experiment. After the generated and dissipated heat balance, the temperature remains basically constant. The temperature data of the motor coil recorded in the experiment and the relationship between the oil viscosity and temperature (Ubbelohde-Walther) [23] are used to obtain the actual viscosity during the experiment (Fig. 9).

The power data collected during the experiment include data on the viscous power, load power and transmission loss. The group 0 experiments are carried out with no compensating oil, and the other conditions remain unchanged. The power data of group 0 include the data of all the power except the viscous power. Therefore, from the power P_1, P_2, P_3, P_4 of groups 1–4, we subtract the power P_0 of group 0 to obtain the data that are related only to the compensating oil viscous power. The viscous power of groups 1–4 is shown in Fig. 10. The higher the kinematic viscosity of the compensating oil

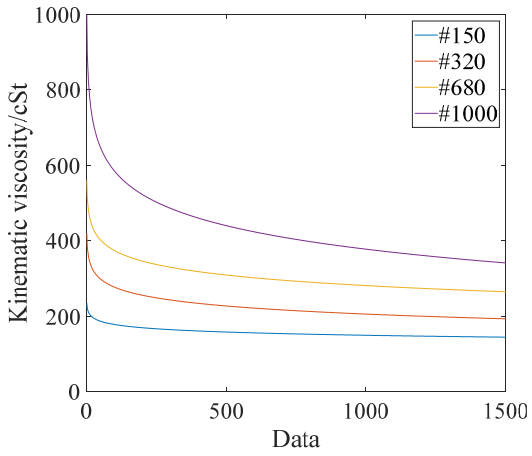

FIGURE 9. Compensating oil viscosity changes.

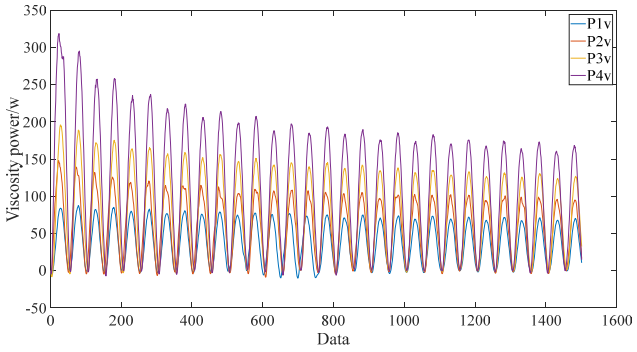

FIGURE 10. Groups 1–4 viscous power.

TABLE 3. Theoretical model error (RMSE/W).

	#150	#320	#680	#1000
Model without T	29.95	46.77	62.41	91.63
Model with T	7.79	10.33	18.22	33.01
Reducing	74%	78%	71%	64%

is, the greater the viscous power that results. During the experiment, as the temperature increases, the viscosity of the compensated oil decreases gradually, and the viscous power decreases gradually.

C. EXPERIMENTAL RESULTS

1) THEORETICAL MODEL EXPERIMENT

The comparison results of the theoretical model and experimental data are shown in Figs. 11–14. Comparisons are made under four different oil viscosities. The theoretical model curves and experimental data points are given in each figure. The theoretical model curves include the model without T (before improvement) and the model with T (after improvement). By comparing the curves and data points in the figure, it can be seen that there is a large error between the model curve (before improvement) and the experimental data points, while the modified model curve largely coincides with the experimental data points.

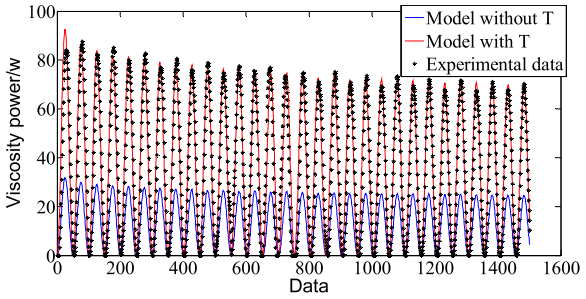

FIGURE 11. Theoretical model experimental results (#150 oil).

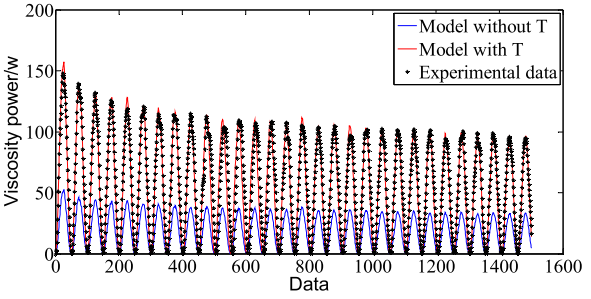

FIGURE 12. Theoretical model experimental results (#320 oil).

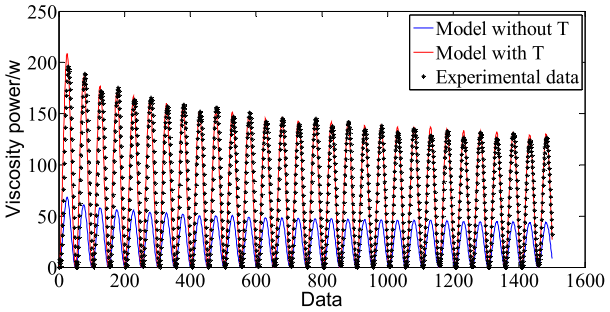

FIGURE 13. Theoretical model experimental results (#680 oil).

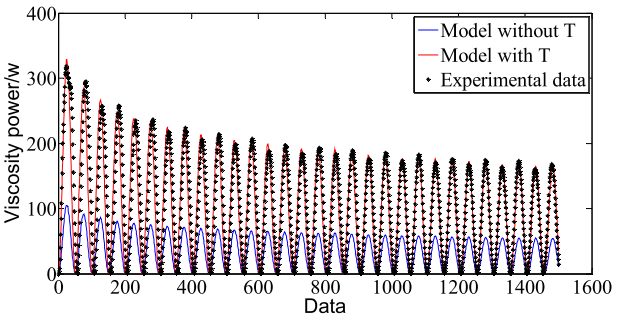

FIGURE 14. Theoretical model experimental results (#1000 oil).

The root mean square error (RMSE) of the theoretical model and experimental data is shown in Table 3. The errors of the modified model are reduced by 74%, 78%, 71% and 64% compared with those before the improvement. It is clearly shown that the modified model can improve the modeling precision in practical problems.

2) VISCOUS POWER OPTIMIZATION EXPERIMENT

After the motor rotor and stator are smoothed, the viscous power experiment is repeated using the experimental

TABLE 4. Viscous power optimization results.

Experimental group number	Compensated oil viscosity /cSt	Average power before optimization /W	Average power after optimization /W	Average power reduction /W
0	No	24.42	25.36	0.94
1	150	36.20 (37.56)	25.35 (24.35)	-10.85 (-13.21)
2	320	54.52 (54.31)	42.62 (43.11)	-11.90 (-11.20)
3	680	75.08 (74.01)	53.27 (53.44)	-22.25 (-20.57)
4	1000	106.02 (101.39)	72.01 (70.11)	-34.01 (-31.28)

installation in 4.1 and the experimental method in 4.2. The optimized experimental results are shown in Table 4. The numbers in brackets in the table represent the results calculated using the modified theoretical model.

It can be seen from experimental group 0 that when there is no compensating oil, the influence of the smoothing process on the motor driving power is very small. This is due to the light weight of the epoxy coating, which is negligible compared with the inertia of the rotor itself. It can be seen from experimental groups 1–4 that the average viscous power decreases after optimization. The greater the viscosity of the compensating oil is, the more clearly the viscous power decreases. When the compensating oil viscosity is 1000 cSt, the average viscous power decreases by 34 W. The calculated results of the theoretical model, in brackets, remain very close to the experimental data.

V. CONCLUSION AND FUTURE WORK

In this paper, a modified viscous power modeling method is proposed based on an analysis of the existing modeling theory and the actual situation of deep-sea electric manipulators. The causes of viscous power loss are further analyzed, and a method for smoothing the rotor and stator surfaces is proposed to optimize the roughness of the fluid clearance geometry and reduce the viscous power loss. Compared with the experimental data, the error of the theoretical modeling method is reduced by an average of 72% after the improvement. This shows that the modified viscous power model proposed in this paper has a higher modeling accuracy for the viscous power of deep-sea electric manipulators. The experimental results of the smoothed rotor and stator of the motor show that the viscous power optimization method has an obvious optimization effect. The viscous loss power decreases by an average of 19.75 W. The theoretical model is also used to analyze the viscous power after the smoothing optimization, and almost the same conclusion is obtained as in the experiment. This shows that the proposed viscous power optimization method can effectively reduce the viscous power loss.

Our future work will focus on the following points: 1) In this paper, the influence of the bearing balls in fluid region 2 is ignored in the theoretical modeling. Bearing ball movement in the compensating oil also produces a certain amount of viscous power, but this aspect of modeling is very difficult. We will examine it next. 2) The deep-sea manipulator studied in this paper is driven directly by the motor and reducer model. There is also a kind of deep-sea electric manipulator that is driven by an electric linear cylinder. The viscous power modeling method for this kind of manipulator is also worth studying.

ACKNOWLEDGMENT

The authors would like to express their gratitude to all their colleagues in the Marine Robotics Department, Shenyang Institute of Automation, Chinese Academy of Sciences.

REFERENCES

[1] E. Zereik, M. Bibuli, N. Mišković, P. Ridao, and A. Pascoal, "Challenges and future trends in marine robotics," *Annu. Rev. Control*, vol. 46, pp. 350–368, 2018, doi: 10.1016/j.arcontrol.2018.10.002.
[2] G. Antonelli, *Underwater Robots*. Berlin, Germany: Springer, 2003.
[3] E. Simetti, G. Casalino, S. Torelli, A. Sperindé, and A. Turetta, "Floating underwater manipulation: Developed control methodology and experimental validation within the TRIDENT project," *J. Field Robot.*, vol. 31, no. 3, pp. 364–385, Jan. 2014, doi: 10.1002/rob.21497.
[4] D. Ribas, P. Ridao, A. Turetta, C. Melchiorri, G. Palli, J. J. Fernandez, and P. J. Sanz, "I-AUV mechatronics integration for the TRIDENT FP7 project," *IEEE/ASME Trans. Mechatronics*, vol. 20, no. 5, pp. 2583–2592, Oct. 2015, doi: 10.1109/tmech.2015.2395413.
[5] R. Capocci, G. Dooly, E. Omerdić, J. Coleman, T. Newe, and D. Toal, "Inspection-class remotely operated Vehicles—A review," *J. Mar. Sci. Eng.*, vol. 5, no. 1, p. 13, Mar. 2017, doi: 10.3390/jmse5010013.
[6] R. D. Christ and R. L. Wernli, *The ROV Manual: A User Guide for Remotely Operated Vehicles*. Oxford, U.K.: Butterworth-Heinemann, 2013.
[7] D. O. B. Jones, "Using existing industrial remotely operated vehicles for deep-sea science," *Zoologica Scripta*, vol. 38, pp. 41–47, Feb. 2009, doi: 10.1111/j.1463-6409.2007.00315.x.
[8] S. Sivčev, J. Coleman, E. Omerdić, G. Dooly, and D. Toal, "Underwater manipulators: A review," *Ocean Eng.*, vol. 163, pp. 431–450, Sep. 2018, doi: 10.1016/j.oceaneng.2018.06.018.
[9] Y. Bai, Q. Zhang, Q. Tian, S. Yan, Y. Tang, and A. Zhang, "Performance and experiment of deep-sea master-slave servo electric manipulator," in *Proc. OCEANS MTS/IEEE SEATTLE*, Oct. 2019, pp. 1–5.
[10] Y. Bai, Q. Zhang, Y. Fan, H. Wang, and A. Zhang, "Research and experiment on viscous friction power loss of deep-sea electric manipulator," in *Proc. OCEANS MTS/IEEE Kobe Techno-Oceans (OTO)*, May 2018, pp. 1–4.
[11] Y. Li, Z. Jiao, T. Yu, and Y. Shang, "Viscous loss analysis of the flooded electro-hydrostatic actuator motor under laminar and turbulent flow states," *Processes*, vol. 8, no. 8, p. 975, Aug. 2020, doi: 10.3390/pr8080975.
[12] D. Pirrà and M. Quadrio, "Direct numerical simulation of turbulent Taylor–Couette flow," *Eur. J. Mech. B/Fluids*, vol. 27, no. 5, pp. 552–566, Sep. 2008, doi: 10.1016/j.euromechflu.2007.10.005.
[13] F. M. White, *Viscous Fluid Flow*. New York, NY, USA: McGraw-Hill Science, 1991.
[14] Q. Wenjuan, Z. Jibin, and L. Jianjun, "Numerical calculation of viscous drag loss of oil-filled BLDC motor for underwater applications," in *Proc. Int. Conf. Elect. Mach. Syst.*, Oct. 2010, pp. 1739–1742.

[15] G. I. Taylor, "Stability of a viscous liquid contained between two rotating cylinders," *Philos. Trans. Roy. Soc. London Ser. A*, vol. 223, nos. 605–615, pp. 289–343, Jan. 1923, doi: 10.1098/rsta.1923.0008.
[16] D. Deng, "A numerical and experimental investigation of Taylor flow instabilities in narrow gaps and their relationship to turbulent flow in bearings," Ph.D. dissertation, Dept. Mech. Eng., Akron Univ., Akron, OH, USA, 2007.
[17] R. J. Donnelly and N. J. Simon, "An empirical torque relation for supercritical flow between rotating cylinders," *J. Fluid Mech.*, vol. 7, no. 3, pp. 401–418, Mar. 1960, doi: 10.1017/s0022112060000177.
[18] F. Wendt, "Turbulente Strömungen zwischen zwei rotierenden konaxialen zylindern," *Ingenieur-Archiv*, vol. 4, no. 6, pp. 577–595, Dec. 1933, doi: 10.1007/bf02084936.
[19] E. Bilgen and R. Boulos, "Functional dependence of torque coefficient of coaxial cylinders on gap width and Reynolds numbers," *J. Fluids Eng.*, vol. 95, no. 1, pp. 122–126, Mar. 1973, doi: 10.1115/1.3446944.
[20] F. Min, Y. Hai, Y. Zhaoyang, W. Wenliang, and M. Chunxu, "Coupling calculation of 3D whole domain steady flow and temperature field for underwater oil-filled brushless DC motors," in *Proc. 22nd Int. Conf. Electr. Mach. Syst. (ICEMS)*, Aug. 2019, pp. 1–6.
[21] J. Zou, W. Qi, Y. Xu, F. Xu, Y. Li, and J. Li, "Design of deep sea oil-filled brushless DC motors considering the high pressure effect," *IEEE Trans. Magn.*, vol. 48, no. 11, pp. 4220–4223, Nov. 2012, doi: 10.1109/TMAG.2012.2204731.
[22] M. Cai, S. Wu, and C. Yang, "Effect of low temperature and high pressure on deep-sea oil-filled brushless DC motors," *Mar. Technol. Soc. J.*, vol. 50, no. 2, pp. 83–93, Mar. 2016, doi: 10.4031/MTSJ.50.2.8.
[23] C. J. Seeton, "Viscosity–temperature correlation for liquids," *Tribology Lett.*, vol. 22, no. 1, pp. 67–78, Apr. 2006, doi: 10.1007/s11249-006-9071-2.

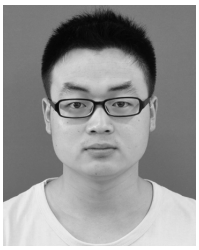

YUNFEI BAI received the B.S. degree in mechatronic engineering from the Changchun University of Science and Technology, Changchun, China, in 2015. He is currently pursuing the Ph.D. degree in mechatronic engineering with the Shenyang Institute of Automation, Chinese Academy of Sciences, Shenyang, China. His research interests include underwater manipulator applications and dexterous operating technology.

QIFENG ZHANG received the B.S. degree in fluid control and automation and the M.S. degree in power engineering from the Harbin Institute of Technology, Harbin, China, in 2001 and 2003, respectively, and the Ph.D. degree in mechatronic engineering from the Shenyang Institute of Automation, Chinese Academy of Sciences, Shenyang, in 2007. He is currently a Professor with the Shenyang Institute of Automation. His research interests include theory and technology for underwater remotely operated vehicle (ROVs) and manipulators.

AIQUN ZHANG received the B.S. degree in mechanical engineering from Northeastern University, Shenyang, China, in 1982. He spent more than 30 years for developing underwater vehicles, first as the Manager with the Marine Robotics Department, Shenyang Institute of Automation, Chinese Academy of Sciences, and more recently as the Engineer-in-Chief with the Institute of Deep-Sea Science and Engineering, Chinese Academy of Sciences. His research interests include overall design for underwater vehicles and technologies for extreme deep-sea exploration.